
PERGAMON

Journal of the Mechanics and Physics of Solids
50 (2002) 2379–2401

JOURNAL OF THE
MECHANICS AND
PHYSICS OF SOLIDS

www.elsevier.com/locate/jmps

Postbuckling of bilaterally constrained rectangular thin plates

B. Roman*, A. Pocheau

IRPHE, Universités Aix-Marseille I & II, 49 rue Joliot-Curie, BP 146, Technopole de Château-Gombert, F-13384 Marseille Cedex 13, France

Received 11 June 2001; received in revised form 4 February 2002; accepted 30 April 2002

Abstract

The post-buckling response of bilaterally constrained thin plates submitted to a height reduction is investigated by a joint experimental–theoretical–numerical study. A detailed determination of the shape of plates is compared to predictions based on modelling the plate as an Elastica and a phase portrait of the system is worked out. An integral relationship for unloaded plates is derived and checked experimentally. The variation of the length of flat contacts with compression is first identified from measurements and then introduced in a virtual work analysis so as to determine the plate reaction. The existence of asymmetric solutions is clarified and the robustness of the Elastica to friction is demonstrated. These results improve the predictions of the Euler model in the fully non-linear regime and validate its relevance beyond the ideal limits of frictionless rod or of frictionless infinite plate on which it is established. They should therefore be useful for addressing buckling in different, albeit close, configurations.

Keywords: A. Buckling; B. Plates; C. Stability and bifurcation elastic materials

1. Introduction

Buckling of thin structures is a widespread phenomenon of such paramount importance for mechanical industry that it has been investigated as early as the foundation times of Solid Mechanics. Its first study dates back to Euler's determination of the buckling load for a pinned–pinned beam (Euler, 1744). Nowadays, it still remains the object

* Corresponding author.
E-mail addresses: benoit.roman@irphe.univ-mrs.fr (B. Roman), alain.pocheau@irphe.univ-mrs.fr (A. Pocheau).

0022-5096/02/$ - see front matter
PII: S0022-5096(02)00028-5

of intense investigation owing to its large implications in many industrial, technological, natural or even biological fields. For instance, the rolling or the levelling of metal sheet in an industrial process or the compliant bearing of journal foils may produce undesirable buckling. Also, the quest for light structures in the aircraft industry has pushed designers to use thinner materials which are therefore more prone to buckle. On the technological side, layered composites may undergo the formation of buckling-induced interlaminar defects, composite steel-concrete constructions may suffer from the buckling of the steel plate used to reinforce the structure and fibre composites or films deposited on a substrate may undergo buckling-induced delamination. More natural manifestations of buckling are also found in thermal buckling of railway tracks, in the pavement buckling induced by earthquakes or in the upheaval failures of rods and runways. More recently, biological implications of buckling are also investigated, for instance in vesicular distortion.

The primary goal of buckling studies consists in understanding the forms and the constraints undergone by thin plates under given external conditions. However, even in its simplest modelizations, this problem comes up to serious difficulties. For instance, although the folding of rods has been modelled for three centuries by Euler's Elastica (Euler, 1744) and despite the fact that its solutions are thoroughly known in terms of jacobian elliptic integrals since more than a century, many of its mechanical properties remain unknown or unsatisfactorily understood in the fully *non-linear* regime. In particular, the problem of shape and tension displayed by thin plates compressed within a box—the so-called *constrained* Elastica—has mostly been addressed by linear methods (Link, 1954; Timoshenko and Gere, 1961) or non-linear ansatz (Paap and Kramer, 1987; Pomeau, 1981) but has mainly resisted more accurate non-linear investigations. Yet, improvements on the understanding of post-buckling in such a simple configuration could provide a valuable basis for gaining insights into more general buckling problems where analytical determinations or detailed comparisons between experiment, theory and simulations are more difficult to achieve.

The purpose of the present study is to improve the modelling and the analysis of compressed thin plates by addressing a regime of *intermediate* complexity: *full* non-linearity but *simple* geometry. For this, thin plates are constrained only *bilaterally* so as to involve only *parallel* folds. However, they are studied in a regime extending *far* from the starting unloaded state and *far* from the buckling bifurcation. Their mechanical response will be addressed below by a joint *experimental–numerical–analytical* study that is dedicated to the following goals: (i) validating Euler's model for quasi-rectangular thin plates, beyond the limits of frictionless rod or of frictionless infinite plate on which it is *a priori* established; (ii) improving the non-linear analysis of Euler's model in the fully non-linear regime. In particular, the implications of friction on plate shape and on plate buckling will be determined and integral relationships for plates will be derived and checked. The experimental set-up is described in Section 2 and Euler's model in Section 3. The analysis of plate form is reported in Section 4 and that of plate constraint in Section 5. Section 6 analyses the implications of friction and a conclusion about the study is drawn in Section 7.

2. Experiment

The experiment aims at achieving compression of bilaterally constrained thin plates, visualizing their fold geometry and measuring their mechanical response. For this purpose, a rectangular plane plate is forced to fit within a parallelepipedic box whose depth Y is varied (Fig. 1). Two kinds of plates will actually be considered throughout the study: the compressing plates of the set-up box and the thin plates to be compressed. To avoid confusion between them, we shall call from now on the thin plates to be compressed, *sheets*, and we shall restrict the designation *plate* to those used to generate compression.

The dimensions and the thickness of the sheet are denoted by L, l, and h, respectively: $h \ll l \prec L$. The sheet is clamped along its *smaller* sides *only* onto the bottom plate of the box. The distance between clamped boundaries, X, is smaller than the length of the sheet, L (Fig. 1a). Therefore, before any load, the sheet is already buckled up to a height labelled Y_1 (Fig. 1a). The buckled sheet is then compressed by simply reducing the distance Y between the upper and bottom plate of the compressing box (Fig. 1c) at fixed lengths X and L. This differs from other configurations studied in the literature where sheet dimensions l, L were kept fixed whereas box dimension X was reduced for a free (Boucif et al., 1991) or an imposed height Y (Daubrée, 1879; Chateau and Nguyen, 1991; Domokos et al., 1997; Chai, 1998). In addition, boundary conditions have been applied here on two opposite sides of the sheet only, rather than on its full perimeter (Boucif et al., 1991), thereby preventing occurrence of folds in the transverse direction as well as material extension. Finally, the geometry of the sheet is a rectangle here ($L/l \approx 2$) instead of a column ($L/l \approx 10$) in the above works. It thus lies plainly in between rods and infinite plates.

The set-up allows the measurement of a *single* component of the elastic reaction force $\mathbf{F}$ of the sheet: the *vertical* component $Q = \mathbf{F}.\mathbf{e}_y$ along the Y-direction $\mathbf{e}_y$ (Fig. 1b,c). This differs from other experimental set-ups where the horizontal component $P = \mathbf{F}.\mathbf{e}_x$ along the X-direction $\mathbf{e}_x$ was measured instead (Boucif et al., 1991; Chai, 1998; Domokos et al., 1997). Although measuring both forces would have been especially interesting, a choice had to be made for practical reasons. It was conditioned by the following consideration: although component P appears of great practical importance, component Q will prove here to be more sensitive to the sheet's shape and thus more

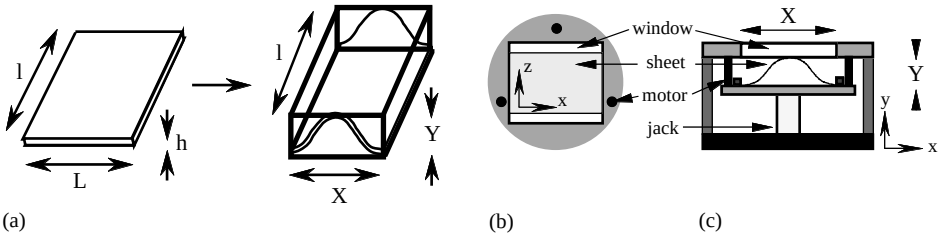

Fig. 1. Sketch of the experimental set-up: (a) initial buckling induced by clamping boundary conditions, (b) top view of the compressing device, (c) side view of the compressing device.

efficient to investigate the correlation between shape and constraint in this system; moreover, being the conjugate of the allowed height Y, component Q will enable us to deal with the work actually transferred to the compressed sheet and thus to address energetic considerations.

In designing the set-up, great care has been devoted to ensure the homogeneous conditions necessary for parallel folds to occur. This especially includes parallelism of the clamping lines and parallelism of the compressing plates of the device. Also, friction along the guiding axes has been minimized so as to allow good accuracy of the reaction force measurement. Finally, clamping conditions have been designed so as to be mostly insensitive to sheet reaction and avoid generation of spurious inhomogeneities on the sheet.

The sheet is clamped on a rigid lower horizontal plate which is guided along three vertical axes by ball bearings. Thanks to a pneumatic jack, this plate can be pushed vertically towards a fixed upper plate in which a glass window is inserted for visualization (Fig. 1c). The distance between plates is controlled by three stepper motors against which the bottom plate is forced to rest. It corresponds to the height Y actually allowed to the sheet. Its accuracy as well as that of the parallelism between compressing plates is provided by the motor accuracy, typically 0.1 μm here.

In steady states, the vertical force developed by the jack is distributed between the three motors and the sheet. Four load gauges located in the bottom plate measure the force exerted by the jack and those received on each of the three motors. The restoring force produced by the sheet on the plates then simply corresponds to the difference between the jack force and the sum of the motor forces. A computer monitors each motor, records force measurement and deduces sheet reaction. The pressure applied to the pneumatic jack is set so that the forces exerted on motors are kept in a reasonable range. There stands the major interest of that jack: helping motors to set accurate distance Y by preventing them from supporting a too large charge from the sheet.

Sheets were made of steel or, more simply, of usual transparent materials, i.e. of polycarbonate. The former were used to perform accurate measurements and the latter to get illustrative pictures with enhanced visibility. No evidence of elastic anisotropy was observed on the mechanical behaviour of polycarbonate sheets. Sheet thickness was $h = 100$ μm for polycarbonate and either $h = 0.1$, 0.2, or 0.3 mm for steel, depending on the desired range for their elastic response. Sheets were enclosed in a box of lateral size $X = 220$ mm. Their lengths were $l = 101$ mm and $L = 233$ mm, except in Section 4.1. Visualization was obtained by looking at the sheets by the side (Fig. 2).

Control parameters of the experiment are the dimensions X and Y of the compressing box together with the sheet length L. In particular as, in a given sheet compression, X and L are kept constant, the crushing history regarding shape and reaction force is parametrized by the geometric ratio L/X. Thanks to a good homogeneity of clamping conditions, all sheet forms have been found invariant along the l-axis. Depending on the control parameters (X, Y, L), they display different kinds of shapes that are shown in Fig. 2. These include curved shapes (Fig. 2a), possibly "suspended" (Fig. 2c) and flat shapes (Fig. 2b).

In the sequel, it will be useful to distinguish different parts of compressed sheets. We shall call a *wrinkle* a sheet part going from one compressing plate to the other and

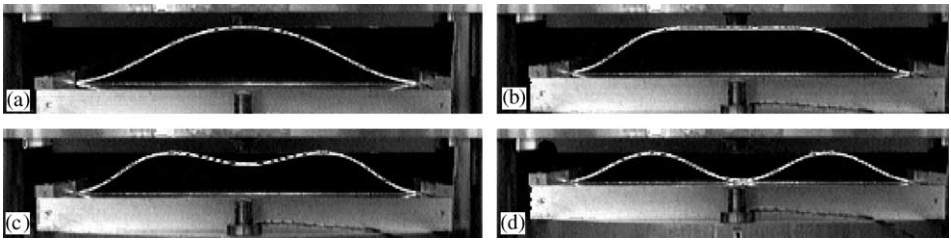

Fig. 2. Transition from one to two wrinkles: side view of polycarbonate sheet, $E \approx 2$ GPa, $X = 220$ mm, $L = 233$ mm, $l = 101$ mm, $h = 1$ mm. *Steady* forms: (a) Line contact: $Y = Y_1$, (b) Planar contact: $Y_p > Y > Y_b$, (c) Post-buckling with free-standing fold: $Y_b > Y > Y_2$, (d) Two wrinkles similar to the one of Fig. 2a: $Y = Y_2$.

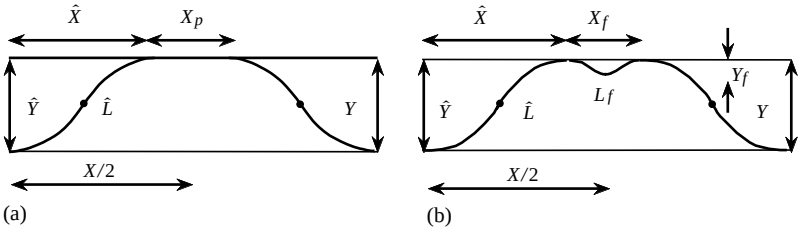

Fig. 3. Sketch and definitions of lengths for a sheet involving: (a) a flat contact part, (b) a free-standing fold. Points correspond to sheets inflexion points I.

returning. Sheets thus involve one wrinkle in Figs. 2a, 2b and two in Fig. 2d. *Fold* will denote a sheet part just connecting one compressing plate to the other. Sheet wrinkles of Figs. 2a, b are thus made of *two* folds. Fold lengths will be denoted $(\hat{X}, \hat{Y}, \hat{L})$ (Fig. 3a). A flat sheet part in contact with compressing plate (Fig. 2b) will be called extended flat contact. We shall label its length X_p (Fig. 3a). Finally, the so-called *free-standing fold* will denote a sheet part starting from one compressing plate but *directly* returning to it. This corresponds to the suspended sheet part of Fig. 2c. We shall denote its lengths (X_f, Y_f, L_f) (Fig. 3b).

3. Model: The Elastica

Although the Elastica model of Euler (1744) addresses the mechanical equilibrium of a *rod*, $l \ll L$, undergoing external force only at its ends, it stands as a natural candidate for modelling quasi-squared thin plates $l \approx L$ folded in a single direction, in particular since it can be shown to also apply to infinite plates, $l \gg L$. The governing equation is

$$EI \frac{d^2\theta}{ds^2} = -p(s)\sin\theta + q(s)\cos\theta, \tag{1}$$

where s is the curvilinear abcissa on the sheet, E Young's modulus, $I(h,l)$ the moment of inertia of the sheet cross-section, θ the angle of the tangent to the sheet with the x-axis and (p,q) the components of the sheet tension $\mathbf{T}$. Euler's equation (1) is submitted here to clamping conditions: $\theta(0)=0$; $\theta(L)=0$. Interestingly, force equilibrium for a sheet at rest implies *constant* tension $\mathbf{T}=(p,q)$ along it: $p(s)=p;(s)=q$. Notice that this differential model hides important conditions to satisfy: the external constraints actually responsible for sheet curvature. In the present case, they consist in forcing a sheet of length L to fit within a box of size X, Y. As they address the *whole* sheet geometry, we shall call them *global* constraints.

3.1. Model assumption

The main assumptions underlying the Euler model refer to the absence of external volumetric forces, to linear elasticity, isometric deformations and planar deformations. The first assumption is equivalent to neglecting gravity compared to elasticity. It is all the more satisfied that the sheet is rigid and curved. The second assumption requires curvature radii to be large compared to thickness h. This condition restricts the allowable height Y to values of order h, i.e. about 200 times smaller than the initial height Y_1. The third assumption means neglecting material extension or, for thin sheets, the Gauss curvature of their mean surface. This is satisfied for rods $l \ll L$ due to their small width but requires for clamped sheets an infinite width $L \ll l$. The fourth assumption turns out to model the material behaviour by a curve lying in a plane and thus to neglect or absorb the mechanical implications of the directions normal to that curve. This can be legitimized for thin sheets $h \ll L$, which are either very wide $l \gg L$ or very narrow $l \ll L$, by analyses of the elasticity equations (Landau and Lifschitz, 1964; Love, 1927) or by invoking regularity of the limits $l/L \to 0$, $l/L \to \infty$ (Barenblatt, 1996). However, its relevance may be questioned on sheets displaying a geometry in between.

3.2. Contact modelling

To model the entire sheet, extension of Elastica to multi-folds must be achieved by specifying the mechanical implications of contact points between sheets and plates. We shall first assume *passive* contacts, i.e. contacts generating *no* friction, *no* moment and involving *no* elastic singularity. At the contact points, this implies continuity of angle (i.e. $\theta=0$), of angle derivative and of tension component p. As for tension component q, notice that, on symmetric wrinkles, right and left folds can be transformed one into the other by reflection $\theta \to -\theta$. This implies that their components q are opposite and thus that contact points provide an impulsion $-2q$ to the sheet. In Section 6, the implications of friction will be addressed by allowing a discontinuity of the constraint p at contact points.

3.3. Properties of the model and formal solutions

We now state the formal solutions to the Elastica and some exact properties of this model that will prove to be useful in the following.

- *Formal solutions*: Bearing formally the same structure as a pendulum equation (Kirchhoff, 1859), Euler's equation possesses formal solutions in terms of partial elliptical integrals. Define parameters $(\bar{\theta}, \omega, k, \phi)$ by

$$q = EI\,\omega^2 \sin(\bar{\theta}); \quad p = EI\,\omega^2 \cos(\bar{\theta}),$$

$$k = \sin\left(\frac{\theta_I - \bar{\theta}}{2}\right); \quad k\sin(\phi) = -\sin(\bar{\theta}/2), \tag{2}$$

where θ_I denotes the angle θ at the inflexion point of the shape (Fig. 3). Introduce the elliptic integrals of the first kind $F(u,k) = \int_0^u [1 - k^2\sin^2(v)]^{-1/2}\,\mathrm{d}v$ and of the second kind $E(\phi,k) = \int_0^\phi [1 - k^2\sin^2(v)]^{1/2}\mathrm{d}v$. Classical integration of Euler's equation (1) then yields, with $\mathscr{F} = F(\pi/2,k) - F(\phi,k)$ and $\mathscr{E} = E(\pi/2,k) - E(\phi,k)$:

$$\hat{L} = 2\int_0^{\hat{L}/2} \mathrm{d}s = \frac{2\mathscr{F}}{\omega},$$

$$\hat{X} = 2\int_0^{\hat{L}/2} \cos(\theta)\,\mathrm{d}s = \frac{2}{\omega}(2\mathscr{E} - \mathscr{F})\cos(\bar{\theta}) - \frac{4}{\omega}\,k\cos(\phi)\sin(\bar{\theta}),$$

$$\hat{Y} = 2\int_0^{\hat{L}/2} \sin(\theta)\,\mathrm{d}s = \frac{2}{\omega}(2\mathscr{E} - \mathscr{F})\sin(\bar{\theta}) + \frac{4}{\omega}\,k\cos(\phi)\cos(\bar{\theta}). \tag{3}$$

- *Symmetry*: Euler's equation is invariant by reflexion $s \to -s$. This means that folds (resp. branches) can satisfy left–right (resp. up–down) symmetry.
- *First integrals*: Euler's equation involves two first integrals, $H(\theta,\dot{\theta})$, $B(\theta,\dot{\theta})$, satisfying $\mathrm{d}H/\mathrm{d}s = 0$, $\mathrm{d}B/\mathrm{d}s = 0$ with

$$H(\theta,\dot{\theta}) = EI\,\frac{\dot{\theta}^2}{2} - p\cos(\theta), -q\sin(\theta), \tag{4}$$

$$B(\theta,\dot{\theta}) = EI[\dot{\theta}(s) - \dot{\theta}(0)] + pY(s) - qX(s), \tag{5}$$

where $[X(s), Y(s)]$ are the coordinates of the sheet point of curvilinear abcissa s. Interpreting s as time makes the Euler equation analogous to a pendulum equation in an inclined gravity field (Kirchhoff, 1859). Within this analogy with dynamical systems, H stands for a hamiltonian and B for a net balance of "impulsion" in between 0 and s.

These first integrals can be used to express the initial curvature of the sheet, $\dot{\theta}_0$, as a function of the tension (p,q) and the constraints $(\hat{X},\hat{Y},\hat{L})$. Equating their values at the initial point $s=0$, $(\theta_0 = 0, \dot{\theta}_0)$ and at the inflexion point I, $(\theta_I, \dot{\theta}_I = 0)$ (Fig. 3), one obtains

$$EI\,\dot{\theta}_0^2 = 4\sin(\theta_I/2)[p\sin(\theta_I/2) - q\cos(\theta_I/2)]$$

$$= 4\sin(\theta_I/2)\omega^2\sin(\theta_I/2 - \bar{\theta}), \tag{6}$$

$$EI\,\dot{\theta}_0 = \frac{p\hat{Y} - q\hat{X}}{2}. \tag{7}$$

- *Dynamical similarity*: In non-dimensional variable $\hat{s} = s/\hat{L}$, Euler's equation reads

$$\frac{\mathrm{d}^2\theta}{\mathrm{d}\hat{s}^2} = -\hat{p}\sin(\theta) + \hat{q}\cos(\theta) \tag{8}$$

  with $\hat{p} = p\hat{L}^2/EI$, $\hat{q} = q\hat{L}^2/EI$. It thus remains an Euler equation but with rescaled forces $\hat{p}$, $\hat{q}$.
- *Curvature energy*: The curvature energy E_c of these fold solutions can be explicitly expressed in terms of tension $T=(p,q)$ and constraints (X,Y,L) (10). For this, notice that hamiltonian (4) equals $H = EI\,\dot{\theta}_0^2/2 - p$ so that

$$E_c = \int_0^{\hat{L}} EI\,\frac{\dot{\theta}^2}{2}\,\mathrm{d}s = \int_0^{\hat{L}} [H + p\cos(\theta) + q\sin(\theta)]\,\mathrm{d}s$$

$$= EI\,\hat{L}\,\frac{\dot{\theta}_0^2}{2} - p(\hat{L} - \hat{X}) + q\hat{Y} \tag{9}$$

  or, following relation (7):

$$E_c = \frac{(p\hat{Y} - q\hat{X})^2}{8}\,\frac{\hat{L}}{EI} - p(\hat{L} - \hat{X}) + q\hat{Y}. \tag{10}$$

  The latter expression is especially interesting since it directly links the curvature energy of folds to the global constraints $(\hat{X},\hat{Y},\hat{L})$ *without* explicit determination of Elastica solutions $\theta(s)$.

3.4. Non-linearity and non-locality

Beyond its formal analogy with a pendulum equation (Kirchhoff, 1859), Euler's equation (1) stands for a markedly different problem. In particular, whereas parameters (p,q) are *fixed* in pendulum dynamics, they are *free* to adjust themselves in the Elastica, so as to provide a solution compatible with global constraints and boundary conditions. In this sense, (p,q) correspond to non-linear *eigenvalues*, similar to front velocity in reaction-diffusion systems for instance.

Solving this kind of problems is usually a hard task, unless there exist integral relationships capable of connecting initial and final conditions (Barenblatt, 1996). In particular, here, the formal solution (3) of Eq. (1) proves to be a non-adequate framework for pointing out the relevant properties of the Elastica. The reason is that most of these properties originate from non-local features of the system which, although included in these exact formal solutions, are not explicitly exhibited. In other words, directly solving the differential equation makes one keep on a local ground which is unsuitable for fully addressing the system. Conversely, using integral relationships makes one rise up to a non-local ground which is more suited to the physics of the system. In particular, expressing from integral relations the compatibility between initial and final conditions often yields an analytic determination of non-linear eigenvalues and, finally, of the solution (Barenblatt, 1996).

In the following, we shall mostly try to follow this track by determining relevant integral relationships from the Elastica's properties. These will follow from the exis-

tence of hamiltonian (4), of the conserved flux (5) along the sheets and of a conserved energy based on Eq. (10).

4. Sheet forms

In this section, we focus attention on some non-linear geometric properties of symmetric wrinkles.

4.1. Unloaded sheets: integral relationship

Consider an unloaded sheet for which $q = 0$. Applying Eqs. (6) and (7), we obtain

$$EI\,\dot{\theta}_0^2 = 4p\sin^2\left(\frac{\theta_I}{2}\right) = \frac{p}{2}\,Y\dot{\theta}_0 \quad \text{or} \quad \sin^2\left(\frac{\theta_I}{2}\right) = \frac{Y}{8R_0}, \tag{11}$$

where $R_0 = \dot{\theta}_0^{-1}$ denotes the curvature radius of the sheet at its top and θ_I the angle of the tangent at its inflexion point.

To test the purely *geometric* relation (11) experimentally, a family of sheets with ratios L/X ranging from 1.016 to 4.4 have been considered. Values of Y, θ_I and R_0 have then been deduced by direct measurement, linear fits and quadratic fits, respectively. Fig. 4a shows quite a good agreement between data and relation (11) on a range of angles θ_I sufficiently large to include fully non-linear variations of $\sin^2(\theta_I/2)$. This provides an indirect but fully non-linear proof of the relevance of the Euler's equation to unloaded sheets.

4.2. Loaded sheets: experimental/numerical agreement

We consider compressed sheets, $q \neq 0$, and compare their forms to those found by numerical integration of Euler's equation within global constraints (X, Y, L). The principle of numerical integration under constraints is reported in the appendix. We stress that it involves no adjustable parameter. Comparison between the two kinds of forms is shown in Fig. 5. It reveals quite a good agreement for line contact sheets. Form agreement is also satisfactory for planar contact sheets but the exact superposition of the curves requires translating the experimental curve onto the numerical curve (Fig. 5). This means that planar contacts preserve form agreement up to a lateral *shift*.

Form agreement between sheets and Elastica solutions supports the relevance of Euler's equation all along the sheets. This suggests that the discrepancy in position noticed in case of planar contacts should likely result from a difference ε between the real experimental boundary conditions $\theta_0 = \varepsilon \ll 1$ and the ideal clamping conditions $\theta_0 = 0$ assumed in simulation. The mechanical origin of this imperfection probably stands in the reaction of the sheet on the clamping device. That noticeable implications only appear in the planar contact regime can be explained by considering the point P where the ideal clamping condition $\theta = 0$ would be recovered by prolongating the sheet for the same tension. We find that this point would be close to the actual boundary condition O in the case of line contact ($PO = O(\varepsilon)$) and comparatively far in the case

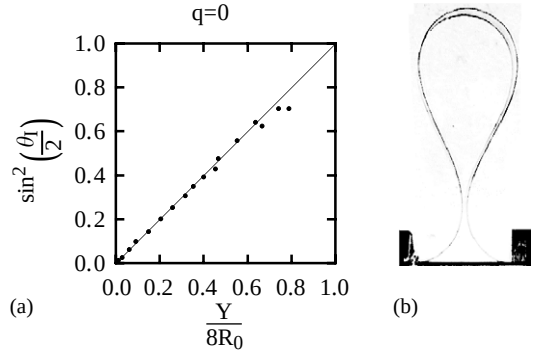

Fig. 4. (a) Experimental measures of $\sin^2(\theta_I/2)$ versus $Y/8R_0$ where θ_I is the angle of the tangent at the inflexion point and R_0 is the radius of curvature at the contact point. The ratio L/X varies in between 1.016 and 4.4. (b) Picture of an unloaded fold with a very large length ratio $L/X = 4.4$.

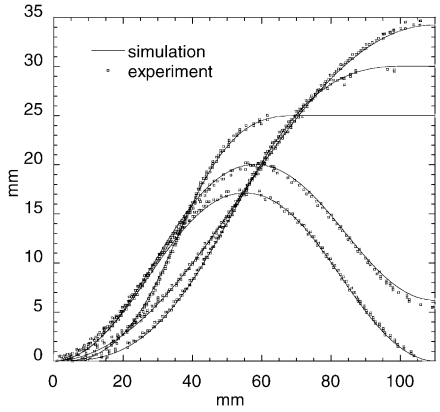

Fig. 5. Comparison of experimental sheet shapes (points) and numerical solutions of Euler's equation (1) (lines). Lengths are $L = 233.3$ mm, $X = 220.5$ mm. The different heights scanned are $Y = 34.5$, 30, 25, 20 and 17.5 mm. A translation of the experimental curve onto the numerical curve is applied in the case of planar contacts. There is no other adjustable parameter, however.

of planar contact ($PO = O(\varepsilon^{1/2})$). Only in the latter case would the difference with ideal clamping conditions be then noticeable.

4.3. Phase portrait

A refined analysis of forms may be achieved by deriving a phase portrait in coordinates $(\theta, \dot{\theta})$ (Holmes et al., 1999). Its interest consists in exhibiting the properties of the *system* from the particular forms of its solutions: the observed compressed *sheets*. Determination of both angle and angle derivative $(\theta, \dot{\theta})$ is naturally provided in numerical simulations since they proceed by integration of Euler's equation. On observed sheets, this requires differentiating the parametric curves $(X(s), Y(s))$ that represent

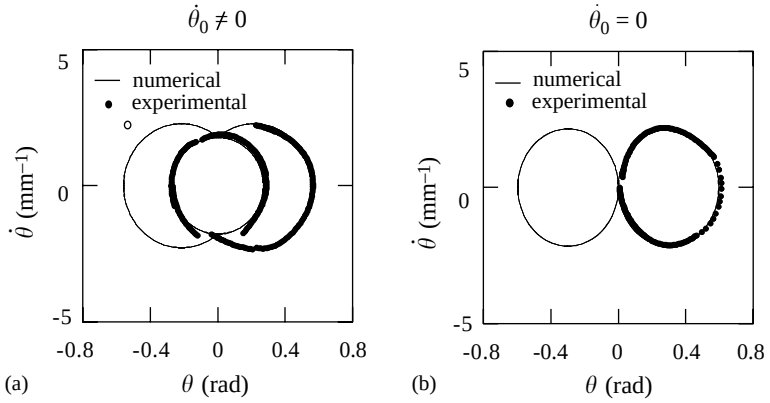

Fig. 6. Phase portrait in coordinates $(\theta, \dot\theta)$ for $X = 220.5$ mm and $L = 231.9$ mm. Thin continuous lines correspond to simulations of Euler's equation (1). Heavy dots are obtained experimentally thanks to polynomial fits of the sheet shape. (a) $Y = 22$ mm: state involving a free-standing fold (Fig. 2c). Ellipses are centered on $(\pm\arctan(q/p), 0)$ for folds and on $(0, 0)$ for the free-standing fold. (b) $Y = 25$ mm: state involving a planar contact (Fig. 2b). Ellipses are centered on $(\pm\arctan(q/p), 0)$.

their forms' cartesian coordinates. To maintain a good signal-to-noise ratio, we have fitted cartesian curves by parts with polynomials of degrees five to seven and differentiated them once (resp. twice) to provide values of $\theta(s)$ (resp. $\dot\theta(s)$). Although data accuracy is weaker than in simulation, it nevertheless enables us to compare the phase portrait obtained by both methods.

Fig. 6 shows the trajectories in phase space $(\theta, \dot\theta)$ typically obtained from experiment and from numerical simulation. Only the left part of sheets has been analysed owing to their left–right symmetry. The agreement between numerical and experimental trajectories is good, whatever the kind of contacts and irrespective of the existence of a free-standing fold. This actually provides a relevant test of Euler's equation for compressed sheets since no adjustable parameters are used at any stage of the procedure.

4.4. Growth of flat domains

In the next section, the evolution of the flat contact length X_p with compression will prove to be a key point for determining the reaction force q of the sheet in the flat contact regime. Measurements of X_p at various height Y are shown in Fig. 7a for a given sheet. They have been obtained by detecting the end points of flat contacts from the sudden change of the reflexion angle of an incident laser beam. Up to measurement accuracy, they show a *linear* variation over a large range of heights Y. Denoting 2α the modulus of its slope and Y_p the height at which flat contact occurs, we get

$$X_p = 2\alpha(Y_p - Y). \tag{12}$$

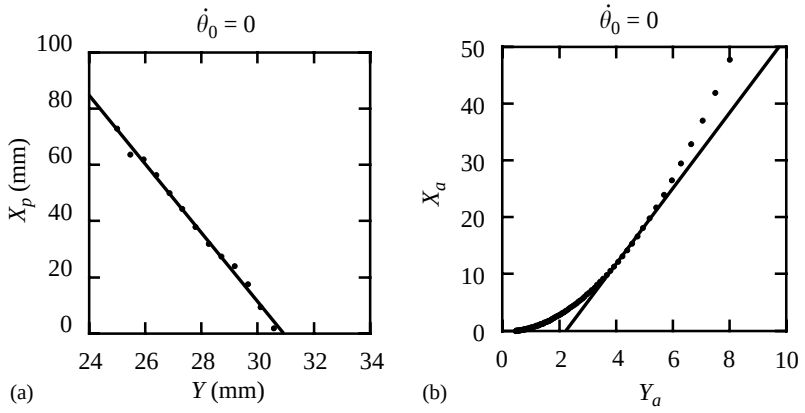

Fig. 7. Approximations in the flat contact regime: (a) Measurements of the evolution of flat contact length X_p as a function of height Y for the same sheet as in Fig. 8. The line is a linear approximation following which $\alpha = 6.10$ and $\rho = 12.06$. (b) Numerical determination of the evolution of fold length $\hat{X}$ with height $\hat{Y}$, both non-dimensionalized by the constant length $(\hat{L} - \hat{X})$: $X_a = \hat{X}/(\hat{L} - \hat{X})$, $Y_a = \hat{Y}/(\hat{L} - \hat{X})$. The line is a linear approximation in the range $4 < Y_a < 5$ in which the regime of Fig. 7a lies. It corresponds to $\alpha = 6.65$, $\rho = 14.87$.

5. Sheet constraints

Despite the relative simplicity of Euler's equation, there does not exist, to our knowledge, explicit analytical expression of force q with respect to height Y and lengths (X, L) on the whole crushing route. In view of this, we first compare below experimental measurements to numerical solutions. We then show that, in the special regime of planar contacts, an approximated but *explicit* relationship $q(X, Y, L)$ can nevertheless be derived from energy conservation. We finally stress the existence of a hysteretic behaviour in the vicinity of buckling, of a negative stiffness of the system in the free-standing fold regime and of a vanishing of constraint q at the end of crushing.

5.1. Mechanical response $q(Y)$

Owing to the dynamical similarity (8) of the Euler equation, constraint q should scale as EI/L^2 with $I = lh^3/12$. This scaling has been tested by comparing reaction q of two sheets made of the *same* material, involving the *same* dimensions except a thickness h *one and a half* bigger for one than for the other. The collapse of the rescaled curves $h^{-3}q(Y)$ shown in Fig. 8a actually evidences both the dynamical similarity of Euler's equation and the scaling law of the moment of inertia I.

Using the above scaling, we now compare the non-dimensionalized reaction force $\tilde{q} = qL^2/EI$ obtained in experiment and simulation. In particular, as experiment involves two folds, only *half* the measured force refers to fold constraint q. Let us introduce $\tilde{Y} = Y/Y_1$ as the height Y non-dimensionalized by the unloaded sheet height

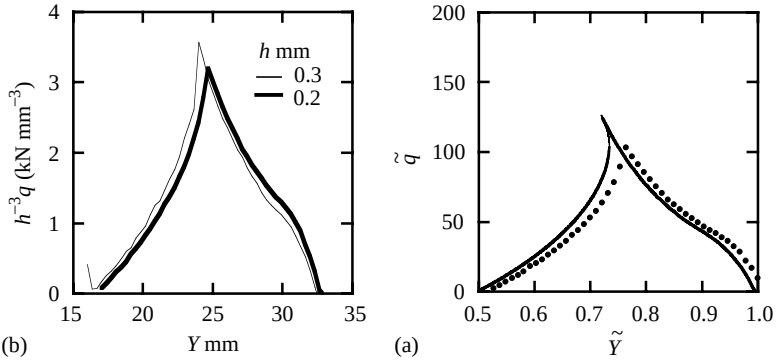

Fig. 8. (a) Collapse of rescaled curves $h^{-3}q(Y)$ for the same material (steel) but two sheet thicknesses, $h = 0.2$ mm and $h = 0.3$ mm. (b) Tension $\tilde{q}$ in non-dimensional variables versus height $\tilde{Y}$. $E \approx 200$ GPa, $h = 0.3$ mm, $X = 220$ mm, $L = 233$ mm, $l = 101$ mm. Scaling used on tension is EI/L^2 with $I = h^3 l/12$. Scaling used on height is $Y_1 = 32.35$ mm. Continuous line (resp. dots) corresponds to numerical integration of Euler's equation (resp. experimental measurements).

Y_1. In non-dimensional variables $(\tilde{Y}, \tilde{q})$, mechanical response q shows in Fig. 8b a good agreement between experiment and simulation, except in the vicinity of the cusp point corresponding to buckling. As no adjustable parameter is used, this provides an additional support for the relevance of Euler's equation.

5.2. Derivation of $q(\hat{X}, \hat{Y}, \hat{L})$ for flat contacts

The constraints $(\hat{X}, \hat{Y}, \hat{L})$ are related to the triplet of variables $(\dot{\theta}_0, p, q)$ by the formal solutions (3) to Euler's equation and by the integral relationships (6) and (7). However, in the general case, the mixing of variables is so intricate that, to our knowledge, no *explicit* expression of tension q as a function of the constraints $(\hat{X}, \hat{Y}, \hat{L})$ can be extracted. Nevertheless, in the special case of flat contacts, i.e. $\dot{\theta}_0 = 0$, we show that integral relationships supplemented by an empirical relation enable the derivation of an approached, but *explicit*, relationship.

To this aim, we first notice that, in the flat contact regime, $\dot{\theta}_0 = 0$, the integral relationships (6) and (7) yield with (2) a number of relations

$$p\hat{Y} = q\hat{X}, \quad \bar{\theta} = \theta_I/2, \quad k = \sin(\theta_I/4), \quad \phi = -\pi/2. \tag{13}$$

On the other hand, we notice that, as $L = 2\hat{L} + X_p$ and $X = 2\hat{X} + X_p$ (Fig. 3a), the length difference $\hat{L} - \hat{X}$ for each fold keeps the same value $(L - X)/2$, *irrespective* of the length X_p of flat contacts. In view of this, we shall use this constant length to non-dimensionalize length X, height Y and constraint q: $X_a = \hat{X}/(\hat{L} - \hat{X})$, $Y_a = \hat{Y}/(\hat{L} - \hat{X})$, $q_a = q(\hat{L} - \hat{X})^2/\mathrm{EI}$. Then, denoting $E \equiv E(\pi/2, k) = -E(-\pi/2, k)$ and $F \equiv F(\pi/2, k) =$

$-F(-\pi/2,k)$ the *complete* elliptic integrals, relation (3) gives, for $\dot{\theta}_0 = 0$:

$$\hat{L} = \frac{4}{\omega} F, \quad \hat{X} = \frac{4}{\omega}[2E - F](1 - 2k^2), \quad \hat{Y} = \frac{4}{\omega}[2E - F]2k(1 - k^2)^{1/2},$$

$$X_a = \frac{\hat{X}}{\hat{L} - \hat{X}} = X_a(k), \quad Y_a = \frac{\hat{Y}}{\hat{L} - \hat{X}} = Y_a(k), \quad \omega = \frac{\Omega(k)}{\hat{L} - \hat{X}}. \tag{14}$$

Here $X_a(.)$ $Y_a(.)$ and $\Omega(.)$ are definite functions of k that can be easily computed.

Relations (2) (13) and (14), show that q_a is related to k and thus, *implicitly*, to $Y_a = Y_a(k)$:

$$q_a = \omega^2(\hat{L} - \hat{X})^2 2k(1 - k^2)^{1/2}, \quad Y_a = Y_a(k). \tag{15}$$

We address below the determination of an approached, but *explicit*, expression of this implicit, but exact, relationship. It is based on the explicit formulation (10) of the curvature energy E_c of folds, following which reaction q can be determined as the gradient of the curvature energy on the Y-direction: $q = (\partial E_c/\partial Y)_{(X,L)}$. However, as p and q vary during height reduction, an additional relation is required to close the problem. In the case of flat contacts, we empirically find it as the law of variation of the contact lengths X_p (12).

In the regime of flat contacts, the curvature energy E_c of the sheet is obtained by adding the curvature energies (9) of each fold, taking into account that the extended flat part involves none. This yields : $E_c = -p(L-X)+2qY$. At fixed (X,L), its variation with height Y reads $\delta E_c = -(L-X)\delta p + 2Y\delta q + 2q\delta Y$. However, this also corresponds to the work done during height reduction: $\delta E_c = -2q\delta Y$ ($-q\delta Y$ for each fold actually). Using the empirical relation (12), the length relation $X = 2\hat{X} + X_p$ (see Fig. 3a) and the integral relationship $pY = q\hat{X}$ (7), we then obtain the ordinary differential equation

$$\frac{dq}{q} = \frac{dq_a}{q_a} = -\frac{dY}{Y} \frac{4Y^2 - \hat{X}_0(L - X)}{2Y^2 - \alpha Y(L - X) + \hat{X}_0(L - X)}, \tag{16}$$

where $\hat{X}_0 = \alpha Y - \hat{X} = \alpha Y_p - X/2$. Integration yields

$$q_a = C \frac{Y_a}{(Y_a^2 - \alpha Y_a + \rho)^{3/2}} \exp\left[-\frac{\alpha}{D} \arctan\left(\frac{2Y_a - \alpha}{D}\right)\right], \tag{17}$$

where C is an integration constant, $\rho = \hat{X}_0/(\hat{L} - \hat{X})$ and $D = (4\rho - \alpha^2)^{1/2}$.

Let us introduce the function $\psi(.)$ which, following (14), implicitly relates the non-dimensional lengths X_a, Y_a in the flat contact regime: $X_a = \psi[Y_a]$. Approximation (12) reduces to linearizing this function: $\psi(Y_a) = \alpha Y_a - \rho$. The graph of function $\psi(.)$, reported in Fig. 7b, shows that, in the range $4 < Y_a < 5$ that is relevant to the measurements of Fig. 7a, the function $\psi(.)$ is hardly distinguishable from its tangent. This validates the linear approximation (12) (17) with $\alpha = 6.65$, $\rho = 14.87$, in good agreement with the values measured from Fig. 7a: $\alpha = 6.10, \rho = 12.06$. The value of the constant C may now be fixed so as to provide equality between the explicit expression (17) and the implicit expression (15) that can be computed from (14). One obtains $C = 0.304$.

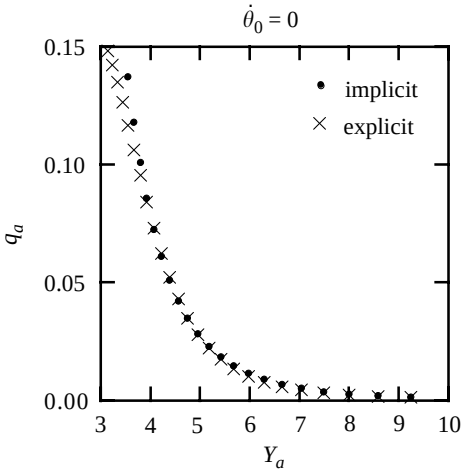

Fig. 9. Comparison between the exact, but implicit, relation $q_a(Y_a)$ (15) and the approximate, but explicit, relation (17).

Fig. 9 shows the graphs of both the exact implicit relation (15) and the approximate explicit relation (17) supplemented with the values of the constants (α, ρ, C) determined above. In the domain where the linear approximation (12) is valid, i.e. $4 < Y_a < 10$, the comparison between them reveals quite a good agreement. Interestingly, energy conservation has thus succeeded in providing here a fine approximation (17) of combinations of elliptic integrals (14) and (15) which, we guess, should be less intuitive from a mathematical point of view.

5.3. Hysteretic behaviour of $q(Y)$

In the flat contact regime, the flat parts can be distributed freely on the sheet since they correspond to rest states $(\theta, \dot{\theta}) = (0, 0)$ of the dynamical system (Roman and Pocheau, 1999). Following this, buckling can occur sooner or later when Y is reduced, depending on whether X_p is concentrated on a single flat part or equally distributed among the different contact regions. In particular, the regimes of flat contacts and of free-standing fold may coexist within a given range of Y. The upper (resp. lower) bound of this range corresponds to the Y-value at which a single flat part (resp. equally long contact parts) buckles.

Having decreased the free-standing fold so that it touches the compressing plate, let us increase depth Y again. A single free-standing fold emerges somewhere at one of the contact points (Fig. 2d). It then reduces amplitude until merging onto a flat part (Fig. 2b). Meanwhile, all other contacts turn to flat contacts since, from (4), the existence of one flat contact, i.e. $(\theta, \dot{\theta}) = (0, 0)$, implies $H = -p$, i.e. $EI\dot{\theta}^2 = p[1 - \cos(\theta)] - q\sin(\theta)$, and thus $\dot{\theta} = 0$ at any other contact point ($\theta = 0$). However, as these other flat contacts arise from line contacts, they all involve by continuity a zero contact length, $X_p = 0$. This means that the free-standing fold ends up on a well defined state: the

largest possible flat part (Fig. 2b). Following this, all experimental data reported here were performed by increasing the box height from a compressed state, so as to obtain well defined reproducible configurations.

5.3.1. Vanishing constraint and negative stiffness

An interesting feature of the mechanical response $q(Y)$ is to be *non*-monotonous (Fig. 8b). Whereas a force q increasing with compression corresponds to the mechanical response of usual systems as common springs, a force q *decreasing* with compression reveals a loss of resistance of the system. Notice that the latter effect occurs within the *linear* regime of elasticity. It thus does not refer to plasticity here but to the change of morphology induced by buckling.

Within this "anti-spring" regime, $\mathrm{d}q/\mathrm{d}Y > 0$, the sheet is unstable under *constant* external force q, and should therefore collapse, possibly exploring a buckling cascade (Roman and Pocheau, 1999). This is actually what happens when the crushing of sheets between parallel plates is performed with the hands. It does not do so within our set-up because height Y is under control. Thanks to this feature, the "anti-spring" regime could be studied here despite its intrinsic instability.

As shown in Fig. 8b, the "anti-spring" regime goes even up to a vanishing of the force q when the free-standing fold just touches a compressing plate (Fig. 2d). This may simply be understood by noticing that the free-standing fold displays *no* tension q. Mechanical response on the Y-direction is then only given by the remaining folds. However, when the free-standing fold just connects compressing plates, it can no longer be distinguished from the remaining folds (Fig. 2d). By continuity, all folds—and therefore the sheet itself—then display a *vanishing* tension q. This, however, is specific to tension q, the tension p showing no vanishing.

6. Robustness to friction

Up to now, we have assumed right–left symmetry for sheets and the absence of friction at the contact points with the compressing plates. However, friction can actually be generated between plates and sheets and asymmetric forms might possibly satisfy constrained Elastica. These possibilities question the agreement obtained so far between experiment, simulation and theory on a *frictionless* and *symmetric* ground. Why friction does not yield noticeable events? Do asymmetrical solutions actually exist? Why are they not naturally encountered along the crushing routes?

On a deeper ground, the above questions raise the problem of the robustness of Euler's model to inevitable friction. In particular, the fact that the frictionless Euler's model works so well in our experiment, despite actual friction, is reminiscent of hydrodynamical configurations where idealistic potential (i.e. inviscid) flows provide an accurate model despite actual viscous dissipation. In hydrodynamic, the reason for this has to be sought in boundary layers. This cannot be invoked here since the existence of integral invariants (e.g. $p(s) = p$) deny a confinement of friction effects (e.g. a change of p) to a definite region.

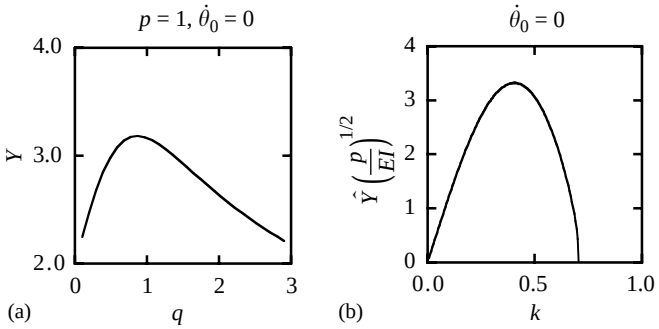

Fig. 10. Graphs showing the existence of couples of solutions involving the same p, the same $\dot{\theta}$ *and* the same Y: (a) line contacts; (b) planar contacts.

Let us address the interplay between asymmetry and friction. As friction generates a tension difference between right and left folds, it forbids their form to be the same: friction *generates* asymmetry. Conversely, as symmetry implies the equality of all characteristics of folds, including their tension component p, it means absence of friction: symmetry *denies* friction. On the other hand, beyond the fact that asymmetry can be induced by friction, one may wonder whether asymmetry does require friction to exist. We give a negative answer below by exhibiting counter-examples of asymmetrical, but frictionless, solutions.

6.1. Existence of asymmetrical frictionless solutions

We index right (resp. left) fold with r (resp. l). Our goal is to construct asymmetric frictionless sheet forms. At contact points, they must involve the same $\dot{\theta}$ and, being frictionless, the same p. Being asymmetric, they involve right and left folds referring to *different* length constraints: $(\hat{X}_\mathrm{r}, \hat{Y}_\mathrm{r}, \hat{L}_\mathrm{r}) \neq (\hat{X}_\mathrm{l}, \hat{Y}_\mathrm{l}, \hat{L}_\mathrm{l})$. However, being confined in between the same plates, they must involve the same height: $\hat{Y}_\mathrm{r} = \hat{Y}_\mathrm{l}$. To satisfy this requirement, we *fix* the parameters $(p, \dot{\theta})$ and we scan the corresponding family of fold solutions of the Elastica by varying another independent variable: q (resp. k) in the case of line (resp. planar) contacts. Within this family, an asymmetrical sheet form is obtained by simply associating folds, each time two of them are found to involve the same height. This gives:

- *Line contacts*: The scan is achieved numerically by varying tension q. A typical family is shown in Fig. 10a. Owing to its bell shape, one gets, for some range of height Y, couples of fold solutions providing asymmetrical, but frictionless, sheets.
- *Planar contacts*: The scan is achieved analytically by varying parameter k in this relation deduced from Eqs. (2) and (14):

$$\hat{Y}(k, p) = 4\left(\frac{p}{EI}\right)^{-1/2}(1-2k^2)^{1/2}[2E-F]2k(1-k^2)^{1/2}. \tag{18}$$

The plot of the function $\hat{Y}(k,1) = (p/EI)^{1/2}\hat{Y}(k,p)$ in Fig. 10b displays a bell-shaped curve showing couples of solutions referring to the same Y. Asymmetrical but frictionless solutions may then be built by associating two different folds of a couple with arbitrarily long flat contact.

6.2. Line contacts and asymmetry

Following the above study, many asymmetrical solutions exist, at least in the frictionless case, and presumably even more when friction is in order. To understand why they are not naturally displayed in our experiment, we consider the actual crushing routes starting from a *definite* initial condition: the *unloaded* state. In unloaded states, tension q vanish and p is the same on each fold since absence of plate means no friction. Moreover, at the point common to right and left folds, curvature and tangent angle are the same. By determinism of Euler's equation (1), this implies equality of fold form : unloaded states can only be *symmetric*.

As compression is set, the clue for understanding the evolution stands in the motion of the contact point C between the sheet and the compressing plates, both on the sheet and on the plates. If C does not move, either on the sheet or on the plates, the length constraints of each fold, $(\hat{X},\hat{Y},\hat{L})$, do not change and thus remain the same for both. However, we have shown that there exists at most one fold of given length $\hat{L}$ satisfying the Elastica in a given box $(\hat{X},\hat{Y})$ (Pocheau and Roman, 2002). Following this unicity property, folds thus involve the same form and the same tension (p,q), so that the sheet *remains* symmetric. Generating sheet *asymmetry* therefore requires *shifting* contact point C, either by gliding, rolling, or both.

- *Gliding motion*: Triggering gliding requires fold tensions p_r, p_l *different enough* for getting off the Coulomb's cone: $|p_\mathrm{r} - p_\mathrm{l}| > \mu(q_\mathrm{r} + q_\mathrm{l})$. However, symmetry itself implies *zero* tension difference: $|p_\mathrm{r} - p_\mathrm{l}| = 0$. Accordingly, gliding cannot stand as a natural way for generating asymmetry from symmetric states: friction *forbids* asymmetry by spontaneous *gliding*.
- *Rolling motion*: Rolling of point C implies that transfer of length on the sheet, $\delta L = L_\mathrm{r} - L_\mathrm{l}$, and on the plates, $\delta X = X_\mathrm{r} - X_\mathrm{l}$, are the same: $\delta L = \delta X = \delta$. On the other hand, following fold uniqueness (Pocheau and Roman, 2002), curvature at the contact point, $\dot{\theta}_\mathrm{C}$, must be a function of the length constraints of the folds. Then, compatibility between right and left folds implies $\dot{\theta}_{\mathrm{C,r}}(X/2+\delta, Y, L/2+\delta) = \dot{\theta}_{\mathrm{C,l}}(X/2-\delta, Y, L/2-\delta)$. This requirement shows that a rolling branch of solution $(\delta \neq 0)$ can be *continuously* taken from the symmetric branch $(\delta = 0)$ only at points satisfying $(\partial\dot{\theta}_\mathrm{C}/\partial X)_{Y,L} + (\partial\dot{\theta}_\mathrm{C}/\partial L)_{X,Y} = 0$. This, at most, can be satisfied on *isolate* points of the crushing routes. Experiment reveals that we did not encounter them or then, did not follow the rolling branch.

6.3. Flat contact and asymmetry

Following the above analysis, we may assume symmetry at the occurence of the flat contact regime. Then, consider the motion of the extremities of the flat contact part

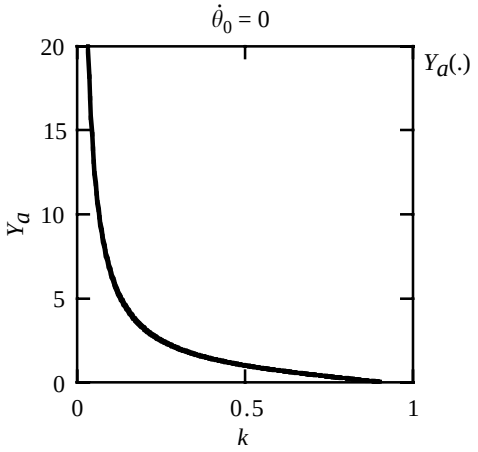

Fig. 11. Graph of function $Y_a(k)$ in the flat contact regime. This function is bijective.

by gliding, rolling or both. Their gliding speed, if any, must be the same since the sheet is inextensible. In particular, flat contact extremities must glide or roll altogether. However, as above, gliding is forbidden until a sufficiently large difference of fold tension p is accumulated. On the other hand, rolling modifies each fold length and lateral extent by the *same* quantities, $dL_r = dX_r$, $dL_l = dX_l$, so that their difference is maintained: $L_r - X_r = L_l - X_l = (L - X)/2$. Then, both folds correspond to the *same* value of $Y_a \equiv \hat{Y}/(\hat{L} - \hat{X})$. However, as this variable is unequivocally linked to k in the flat contact regime (Fig. 11), it solely governs the form of folds involving flat contacts. Accordingly, the two folds of the sheet must then be the *same*. Apart from the distribution of flat parts (which changes in case of different rolling velocities), sheet thus remains symmetric.

6.4. Free-standing fold: evidence of friction

At its birth, i.e. at buckling, a free-standing fold involves a length L_f equal to its lateral extent $X_f : L_f - X_f = 0$. At its end, i.e. when further compression brings it into contact with the opposite plate, its length (resp. lateral extent) is half that of the sheet (resp. box): $(L_f - X_f) = (L - X)/2$. Its length difference $(L_f - X_f)$ thus necessarily increases during compression. This requires gliding and, therefore, friction.

Friction for free-standing fold is evidenced in Fig. 12a by plotting force q over a cycle obtained by compressing until the free-standing fold touches the opposite plate and return. The net area of the cycle means that the operator has furnished a net work to return to the same state. This reveals friction on this route. In Fig. 12b, the same procedure is applied to the regimes of line contacts and planar contacts. There, the *same* points are found on the compression path and return, showing absence of friction in these regimes.

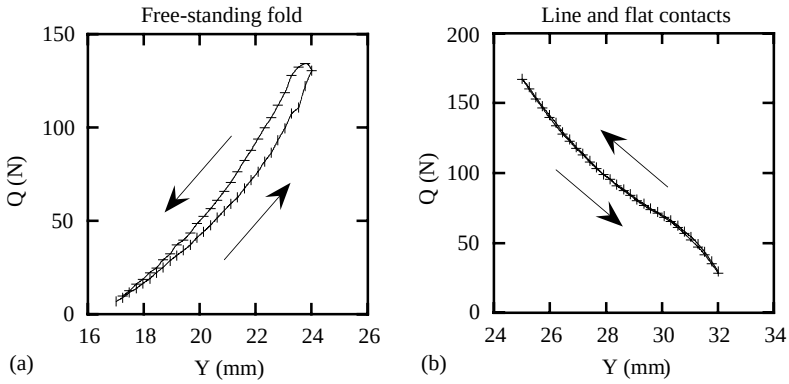

Fig. 12. Cycles showing small dissipation in the case of free-standing fold (a) and conservative behaviour in the case of line contact and flat contact (b). Experimental data are shown by vertical bar (increasing Y) and horizontal bars (decreasing Y).

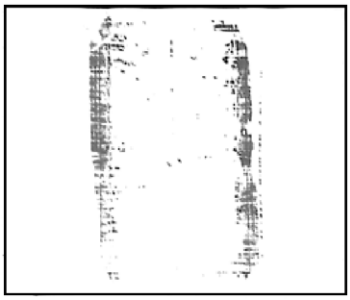

Fig. 13. Picture of a polycarbonate sheet. The upper compressing plate was covered with a coloured powder. This powder could be sticked to the sheet in the area involving sliding between the two surfaces. Notice the absence of sliding in the central region, but the existence of some in the domain where the free-standing fold was in contact with the upper compressing plate.

Friction is directly evidenced in Fig. 13 by covering compressing plate with a coloured ink and performing sheet compression. As checked directly, sticking of ink onto the sheet could not arise by rolling but by gliding. Starting from the unloaded state, two symmetric bands on the sheet were nevertheless marked with ink. They corresponded neither to the location of the contact point in the line contact regime, nor to those displayed in the flat contact regime but to those involved in the free-standing fold regime. This confirms gliding in this sole last regime.

We nevertheless notice that, as tension q goes back to zero when the free-standing fold approaches the compressing plate, friction vanishes again at the end of this regime. This makes the frictionless Euler model recover its validity for further compression, as shown in a study of buckling cascade (Roman and Pocheau, 1999).

6.5. Structural stability of Euler's Elastica with respect to friction

The above results reveal an interesting robustness of Euler's modelization to friction. Friction indeed widely opens the set of solutions of constrained Elastica by introducing an additional degree of freedom: the impulsion induced at contact points. However, it also generates a threshold, the Coulomb angle, which prevents symmetric states to experience gliding under compression. Thanks to fold uniqueness (Pocheau and Roman, 2002), this reduces the opportunity of dissymmetrizing sheet forms to at most isolate points on the line contact regime. In turn, the fact that the sheet remains symmetric eventually denies friction.

Friction thus surprisingly stabilizes frictionless symmetric routes. Owing to this positive role, it prevents the natural occurence of the many states that it nevertheless allows. This is the reason why the frictionless Euler model remains relevant even in the real frictional world.

7. Conclusion

The response of bilaterally constrained thin plates to height reduction has been investigated by a joint experimental–theoretical–numerical study. An aspect ratio intermediate between those of a rod and of an infinite plate has been chosen so as to better fit with practical applications regarding layered composites or industrial processing of sheet metal or of journal foil. Euler's model has been chosen to model the plate responses despite their finite aspect ratio and despite friction. Attention has then been paid to attest its relevance and to investigate its properties in the non-linear regime.

The shape of plates and their elastical constraints at a given compression as well as their changes with compression have revealed quite a good agreement between experiment, numerical simulation and analysis. This extends the practical validity of the Elastica model from the "degenerate" geometry of rods or infinite plates to which it is a priori dedicated, to the intermediate asymptotic regime of plates with *finite* aspect ratio. On the other hand, the global structure of the Elastica has been revealed by pointing out its phase portrait experimentally and by showing evidence of its similarity. The sensitivity of the model to boundary conditions has been analysed and integral relationships regarding forms and reaction forces have been derived and checked against experiment. In particular, elastical reactions have been derived in the flat contact regime from the integral expression of the curvature energy and from the phenomenological evolution of flat contact lengths. At last, Euler's model has been shown to be robust with respect to friction, a result that explains its widespread relevance to practical situations where friction is inevitably involved.

The improvement of the non-linear properties of constrained rectangular thin plates is interesting not only for the situations where this configuration is encountered but also for those where slight modifications regarding plate initial curvature, fold axis curvature, thermal gradient or shear prevent using integral relationships. Comparing their elastical response to those displayed in Euler buckling would then be quite instructive for extending the detailed understanding of buckling to more natural situations. In this

spirit, the present study may be viewed as providing a detailed basis for getting valuable insights into more complex buckling problems, in addition to its direct usefulness to situations where finite aspect ratio plates show parallel folds (Iseki et al., 1989; Hesmat et al., 1983; Chou and Rhodes, 1997; Nordstrand and Carlsson, 1997).

Appendix. Numerical method

For simplicity, lengths are scaled so that $L \equiv 1$. The integration of Euler's equation (1) is achieved by the Runge–Kutta method. However, eigenvalues (p,q) and initial conditions $(\theta_0, \dot{\theta}_0)$ have to be given so as to deduce the form $\theta(s)$ and finally conclude whether global constraints (X,Y) are satisfied for the sheet length $L \equiv 1$. Agreement between prescribed variables and global constraints can be sought by applying a shooting technique, as documented in numerous numerical works (Patricio et al., 1998; Plaut et al., 1999). Differences arise regarding the nature of the contacts between sheet and plate.

For a line contact, we start with an initial guess on $(p,q,\dot{\theta}_0)$, the initial condition $\theta_0 = 0$ being imposed. A program provides the form $\theta(s)$ from which the cartesian coordinates $[x(s), y(s)]$ of a point of curvilinear abcissa s are deduced by integration. Satisfying the global constraints then reduces to finding the *zero* of the function which links $(p,q,\dot{\theta}_0)$ to $[x(1/2)-X/2, y(1/2)-Y, \theta(1/2)]$. Here, the third condition $\theta(1/2)=0$ specifies that the boundary $s=1/2$ is actually a contact point with the upper plate. This stands as a classical numerical problem which can be easily solved provided a suitable initial guess is taken. In particular, to find out a continuous branch of solution, a relevant method consists in taking the solution for a given height Y as a guess for determining the solution for a neighbor value Y'.

For a plane contact, the quest for the solution is slightly modified in the sense that the initial condition $\dot{\theta}_0$ is given, $\dot{\theta}_0 = 0$, but that the length X_p of the flat contact is unknown. The guess underlying the integration then involves the variables (p,q,X_p). Denoting $\sigma_p=(1-X_p)/2$ the length of each fold, the problem then turns out determining the *zero* of the function which links (p,q,X_p) to $(x(\sigma_p)-(X-X_p)/2, y(\sigma_p)-Y, \theta(\sigma_p))$. for the initial condition $\theta_0 = \dot{\theta}_0 = 0$.

Finally, in regimes involving a free-standing fold, a similar procedure enables the form and tension of the sheet to be found.

References

Barenblatt, G.I., 1996. Scaling, Self-Similarity and Intermediate Asymptotics. Cambridge University Press, Cambridge.

Boucif, M., Weisfreid, J.E., Guyon, E., 1991. Experimental study of wavelength selection in the elastic buckling instability of thin plates. Eur. J. Mech. A/Solids 10 (6), 641–661.

Chai, H., 1998. The post-buckling response of a bi-laterally constrained column. J. Mech. Phys. Solids 46 (7), 1155–1181.

Chateau, X., Nguyen, Q.S., 1991. Buckling of elastic structures in unilateral contact with or without friction. Eur. J. Mech. A/Solids 10 (1), 71–89.

Chou, S., Rhodes, J.A., 1997. Review and compilation of experimental results on thin-walled structures. Comput. Struct. 65 (1), 47.

Daubrée, A., 1879. Etudes synthétiques de géologie Expérimentale. Dunod, Paris, 1879, pp. 288–300.

Domokos, G., Holmes, P., Royce, B., 1997. Constrained Euler buckling. J. Nonlinear Sci. 7, 281–314.

Euler, L., 1744. Additamemtum I de curvis elasticis, Methodus inveniendi lineas curvas maximi minimivi proprietate gaudentes. In: Opera Omnia I, Vol. 24. Bousquet, Lausanne, pp. 231–297.

Hesmat, H., Walowit, J.A., Pinkus, O., 1983. Analysis of gas lubricated compliant thrust bearings. J. Lubrication Technol. 105, 638–646.

Holmes, P., Domokos, G., Schmitt, J., Szeberényi, I., 1999. Constrained Euler buckling: an interplay of computation and analysis Comput. Methods Appl. Mech. Eng. 170, 175–207.

Iseki, H., Sowerby, R., Bhattacharyya, D., Gatt, P., 1989. A theoretical and experimental study of a curved strip compressed by a flat plate. J. Appl. Mech. 56, 96–104.

Kirchhoff, G., 1859. Über das gleichgewicht und die bewegung eines unendlich dünen elastischen stabes. J. Math. 56, 285–313.

Landau, L.D., Lifschitz, E.M., 1964. Theory of Elasticity. Pergamon Press, New York.

Link, H., 1954. Über den geraden knickstab mit begrenzter durchbiegung. Ing. Arch. 22, 237–250.

Love, A.E.H., 1927. Mathematical Theory of Elasticity. Cambridge University Press, Cambridge.

Nordstrand, T.M., Carlsson, L.A., 1997. Evaluation of transverse shear stiffness of structural core sandwich plates. Compos. Struct. 37, 145–153.

Paap, H., Kramer, L., 1987. Wavenumber restriction in systems with discontinuous nonlinearities and the buckling instability of plates. J. Phys. 48, 1471–1478.

Patricio, P., Adda-Beddia, M., Ben Amar, M., 1998. An elastica problem: instabilities of an elastic arch Physica D 124, 285–295.

Plaut, R., Suherman, S., Dillard, D., Williams, B., Watson, L., 1999. Deflections and buckling of a bent elastica in contact with a flat surface. Int. J. Solids Struct. 36, 1209–1229.

Pocheau, A., Roman, B., 2002. Unicity of solutions for constrained elastica. Physica D, submitted for publication.

Pomeau, Y., 1981. Non-linear pattern selection in a problem of elasticity. J. Phys. Lett. 42, L1–L4.

Roman, B., Pocheau, A., 1999. Buckling cascade of thin plates: forms, constraints and similarity. Europhys. Lett. 46 (5), 602–608.

Timoshenko, S., Gere, J., 1961. Theory of Elastic Stability. McGraw-Hill, New York.